

Powell-Sabin splines with boundary conditions for polygonal and non-polygonal domains

Hendrik Speleers

Paul Dierckx

Stefan Vandewalle

Report TW 452, March 2006



Katholieke Universiteit Leuven
Department of Computer Science
Celestijnenlaan 200A – B-3001 Heverlee (Belgium)

Powell-Sabin splines with boundary conditions for polygonal and non-polygonal domains

Hendrik Speleers

Paul Dierckx

Stefan Vandewalle

Report TW 452, March 2006

Department of Computer Science, K.U.Leuven

Abstract

Powell-Sabin splines are piecewise quadratic polynomials with a global C^1 -continuity, defined on conforming triangulations. Imposing a boundary condition on such a spline leads to a set of constraints on the spline coefficients. First we discuss boundary conditions defined on a polygonal domain, before we treat boundary conditions on a general curved domain boundary. We consider Dirichlet and Neumann conditions, and we show that a particular choice of the PS-triangles at the boundary can greatly simplify the corresponding constraints. Finally, we consider an application where the techniques developed in this paper are used: the numerical solution of a partial differential equation by the Galerkin and collocation method.

Keywords : Powell-Sabin splines, boundary conditions

AMS(MOS) Classification : Primary : 41A29, Secondary : 65N30, 41A15

Powell-Sabin splines with boundary conditions for polygonal and non-polygonal domains

Hendrik Speleers, Paul Dierckx and Stefan Vandewalle

*Department of Computer Science, Katholieke Universiteit Leuven
Celestijnenlaan 200A, B-3001 Leuven, Belgium*

Abstract

Powell-Sabin splines are piecewise quadratic polynomials with a global C^1 -continuity, defined on conforming triangulations. Imposing a boundary condition on such a spline leads to a set of constraints on the spline coefficients. First we discuss boundary conditions defined on a polygonal domain, before we treat boundary conditions on a general curved domain boundary. We consider Dirichlet and Neumann conditions, and we show that a particular choice of the PS-triangles at the boundary can greatly simplify the corresponding constraints. Finally, we consider an application where the techniques developed in this paper are used: the numerical solution of a partial differential equation by the Galerkin and collocation method.

Keywords: Powell-Sabin splines, boundary conditions

AMS classification: 41A29, 65N30, 41A15, 65D07

1 Introduction

In computer-aided geometric design and scientific computing it is often important that a function or surface preserves certain geometric properties, e.g. boundary conditions. Chui and Schumaker [3] were the first to investigate spaces of piecewise polynomial surfaces with boundary conditions. They considered splines on a rectangle partitioned into subrectangles, with vanishing normal derivatives on the boundary. In [3], the dimension of these spaces was computed and an appropriate local basis was constructed. This study was continued in [4, 5] for spaces of boundary constrained piecewise polynomials on type-1 and type-2 triangulations. Such triangulations are constructed by subdividing rectangular partitions of a rectangular domain by using the diagonals.

Shi *et al.* [15] studied the dimension and suggested a basis for the so-called Powell-Sabin (PS-) spline space subject to homogeneous Dirichlet and Neumann boundary conditions. Powell-Sabin splines are piecewise quadratic polynomials with a global C^1 -continuity, defined on conforming triangulations. Willemans and Dierckx used in [19] constrained Powell-Sabin splines for smoothing scattered noisy measurement data. Speleers *et al.* [17] treated Dirichlet boundary conditions, i.e. $u(x, y) = f(x, y)$, and Neumann boundary conditions, i.e. $\frac{\partial}{\partial n}u(x, y) = g(x, y)$, with arbitrary boundary functions $f(x, y)$ and $g(x, y)$, imposed on Powell Sabin splines in the context of a finite element method. The set of corresponding constraints on the PS-spline coefficients are very simple by a particular choice of the basis functions at the boundary.

Another technique to deal with homogeneous Dirichlet conditions consists of multiplying the basis functions with a positive weight function that vanishes on the boundary of the domain. This idea became successful in connection with the R-function method of Rvachev [13]. It is very effective in combination with the classical tensor-product splines [14, 10]: a homogeneous boundary condition

defined on an arbitrary curved boundary can be exactly imposed without loss of the approximation power of the splines.

In this paper, we discuss a new approach for the treatment of Dirichlet and Neumann conditions on (a part of) the boundary with Powell-Sabin splines. Instead of choosing the basis functions at the boundary differently for each type of condition, as in [17], we now derive an approach that allows a uniform treatment for all cases. It results in a basis that is more stable, and that can be constructed in advance, irrespective of the particular application. We also treat the situation where the boundary conditions are no longer defined on the polygonal boundary of the triangulation. This case will enable an efficient and accurate boundary condition representation on general curved boundaries.

The paper is organized as follows. Section 2 reviews the definition of the Powell-Sabin spline space, and recalls the construction of a normalized B-spline basis. In section 3 we discuss some general characteristics of the Powell-Sabin spline at the boundary. Section 4 addresses the treatment of different boundary conditions defined on the boundary of the triangulation. In section 5 boundary conditions on non-polygonal domains are considered. In each of those cases, we show that a particular choice of the Powell-Sabin basis functions associated with the boundary vertices can greatly simplify the boundary constraints. We illustrate our treatment of the boundary conditions using the Poisson equation. Finally, in section 7 we end with some concluding remarks.

2 Powell-Sabin splines

2.1 The space of Powell-Sabin splines

Consider a simply connected subset $\Omega \in \mathbb{R}^2$ with polygonal boundary $\partial\Omega$. Assume a conforming triangulation Δ of Ω is given, consisting of t triangles $\rho_j, j = 1, \dots, t$, and having n vertices $V_k, k = 1, \dots, n$. A triangulation is conforming if no triangle contains a vertex different from its own three vertices.

The Powell-Sabin (PS-)refinement Δ^* of Δ partitions each triangle ρ_j into six smaller triangles with a common vertex Z_j . This partition is defined algorithmically as follows:

1. Choose an interior point Z_j in each triangle ρ_j . If two triangles ρ_i and ρ_j have a common edge, then the line joining Z_i and Z_j should intersect the common edge at some point R_{ij} .
2. Join each point Z_j to the vertices of ρ_j .
3. For each edge of the triangle ρ_j
 - (a) which is common to a triangle ρ_i : join Z_j to R_{ij} ;
 - (b) which belongs to the boundary $\partial\Omega$: join Z_j to an arbitrary point R on that edge.

In the sequel, we will take R such that the line Z_j - R is normal to the boundary edge. This position of R will reduce the computational complexity in the treatment of Neumann boundary conditions. Choosing Z_j as the incentre of ρ_j ensures R is situated between the two boundary vertices of ρ_j . In Figure 1(a) such a PS-refinement of a given triangulation is drawn in dashed lines.

The space of piecewise quadratic polynomials on Δ^* with global C^1 -continuity is called the Powell-Sabin spline space:

$$S_2^1(\Delta^*) = \left\{ s \in C^1(\Omega) : s|_{\rho_j^*} \in \Pi_2, \rho_j^* \in \Delta^* \right\}. \quad (2.1)$$

Powell and Sabin [12] proved that the following interpolation problem

$$s(V_l) = f_l, \quad \frac{\partial s}{\partial x}(V_l) = f_{x,l}, \quad \frac{\partial s}{\partial y}(V_l) = f_{y,l}, \quad l = 1, \dots, n. \quad (2.2)$$

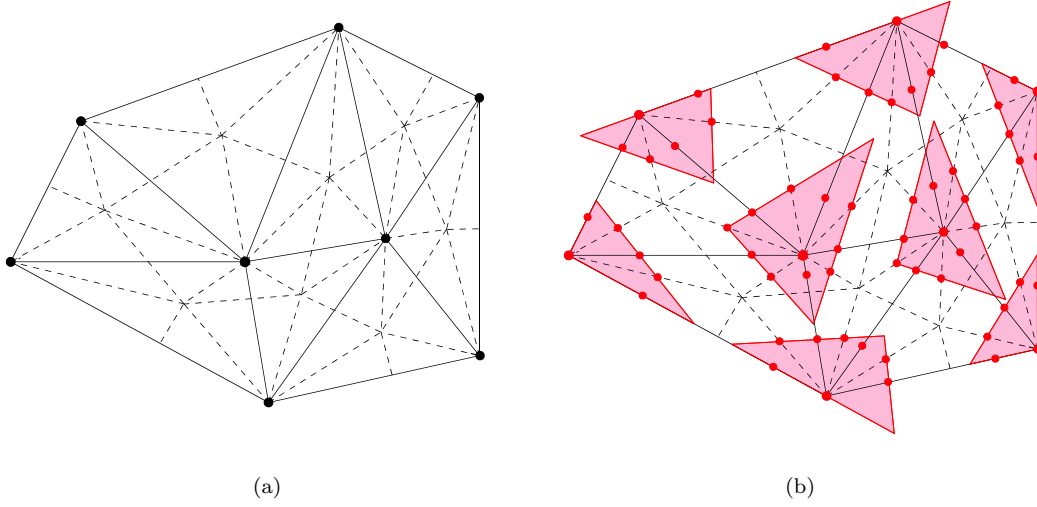


Figure 1: (a) A PS-refinement Δ^* (dashed lines) of a given triangulation Δ (solid lines); (b) the PS-points (bullets) and a set of suitable PS-triangles (shaded).

has a unique solution $s(x, y) \in S_2^1(\Delta^*)$ for any given set of n $(f_l, f_{x,l}, f_{y,l})$ -values. It follows that the dimension of the Powell-Sabin spline space $S_2^1(\Delta^*)$ is equal to $3n$.

2.2 A normalized B-spline representation

Dierckx *et al.* [9] considered a suitable representation for Powell-Sabin splines. With each vertex V_i three linearly independent triplets $(\alpha_{i,j}, \beta_{i,j}, \gamma_{i,j})$, $j = 1, 2, 3$ are associated. The B-spline $B_i^j(x, y)$ can be found as the unique solution of interpolation problem (2.2) with all $(f_l, f_{x,l}, f_{y,l}) = (0, 0, 0)$ except for $l = i$, where $(f_i, f_{x,i}, f_{y,i}) = (\alpha_{i,j}, \beta_{i,j}, \gamma_{i,j}) \neq (0, 0, 0)$. It is easy to see that this B-spline has a local support: $B_i^j(x, y)$ vanishes outside the so-called molecule M_i of V_i , meaning the union of all triangles containing V_i . Every Powell-Sabin spline can then be represented as

$$s(x, y) = \sum_{i=1}^n \sum_{j=1}^3 c_{i,j} B_i^j(x, y). \quad (2.3)$$

The basis forms a convex partition of unity on Ω if

$$B_i^j(x, y) \geq 0, \quad \text{and} \quad \sum_{i=1}^n \sum_{j=1}^3 B_i^j(x, y) = 1, \quad (2.4)$$

for all $(x, y) \in \Omega$. This property, together with the local support of the Powell-Sabin B-splines, lies at the basis of their computational effectiveness in many application domains, see [9, 18, 11, 17]. In [8] Dierckx has presented a geometrical way to derive and construct such a normalized basis:

1. For each vertex $V_i \in \Delta$, identify the corresponding PS-points. These points are defined as the midpoints of all edges in the PS-refinement Δ^* containing V_i . The vertex V_i itself is also a PS-point. In Figure 1(b) the PS-points are indicated as bullets.
2. For each vertex V_i , find a triangle $t_i(Q_{i,1}, Q_{i,2}, Q_{i,3})$ containing all the PS-points of V_i . The triangles t_i , $i = 1, \dots, n$ are called PS-triangles. Note that the PS-triangles are not uniquely

defined. Figure 1(b) shows some PS-triangles. One possibility for their construction [8] is to calculate a triangle of minimal area. Computationally, this problem leads to a quadratic programming problem. It turns out that other choices are more appropriate in the treatment of boundary conditions. The fact that the PS-triangle t_i contains the PS-points of the vertex V_i guarantees the positivity property of (2.4).

3. The three linearly independent triplets $(\alpha_{i,j}, \beta_{i,j}, \gamma_{i,j})$, $j = 1, 2, 3$ are derived from the PS-triangle t_i of a vertex V_i as follows:

- $\alpha_i = (\alpha_{i,1}, \alpha_{i,2}, \alpha_{i,3})$ are the barycentric coordinates of V_i with respect to t_i ,
- $\beta_i = (\beta_{i,1}, \beta_{i,2}, \beta_{i,3})$ and $\gamma_i = (\gamma_{i,1}, \gamma_{i,2}, \gamma_{i,3})$ are the coordinates of the unit barycentric directions, in x - and y -direction respectively, with respect to t_i .

We define the PS-control points as $C_{i,j} = (Q_{i,j}, c_{i,j})$ and PS-control triangles as $T_i(C_{i,1}, C_{i,2}, C_{i,3})$. One can easily prove that the PS-control triangle T_i is tangent to the surface $z = s(x, y)$ at the vertex V_i .

3 The characterization of a PS-spline at the boundary

In this section we discuss some characteristics of a Powell-Sabin spline and its normal derivative at the boundary. We show how they can be described by particular one-dimensional splines, and we derive the relation between these splines. We will often need to distinguish two boundary situations, i.e., a straight boundary edge intersection angle and an angle different from π . We will refer to those cases as case I and case II respectively.

Suppose that V_i , V_j and V_k are counter-clockwise successive boundary vertices. In case II, a relation exists between the tangential and normal derivatives at vertex V_j . The tangential directions in clockwise and counter-clockwise direction can easily be found as

$$\bar{t}_{ij} = \frac{V_i - V_j}{\|V_i - V_j\|}, \quad \text{and} \quad \bar{t}_{kj} = \frac{V_k - V_j}{\|V_k - V_j\|}. \quad (3.1)$$

Let \bar{n}_{ij} and \bar{n}_{kj} be the outward normal directions on the boundary edges V_i - V_j and V_j - V_k respectively. Because of the inherent C^1 -continuity of the Powell-Sabin spline, the normal and tangential derivatives are related. The following relations can be shown to hold at vertex V_j

$$\frac{\partial}{\partial \bar{t}_{kj}} = \cos(\theta) \frac{\partial}{\partial \bar{t}_{ij}} - \sin(\theta) \frac{\partial}{\partial \bar{n}_{ij}}, \quad (3.2a)$$

$$\frac{\partial}{\partial \bar{n}_{kj}} = -\sin(\theta) \frac{\partial}{\partial \bar{t}_{ij}} - \cos(\theta) \frac{\partial}{\partial \bar{n}_{ij}}, \quad (3.2b)$$

with θ the angle between the vectors \bar{t}_{ij} and \bar{t}_{kj} in the interior of the domain, as illustrated in Figure 2. For a case I vertex, where $\theta = \pi$, we have that $\frac{\partial}{\partial \bar{t}_{ij}} = -\frac{\partial}{\partial \bar{t}_{kj}}$ and $\frac{\partial}{\partial \bar{n}_{ij}} = \frac{\partial}{\partial \bar{n}_{kj}}$. Another special case is a right boundary edge intersection angle, i.e. with $\theta = \pi/2$ or $3\pi/2$. The tangential and normal derivatives are then obviously related as $\frac{\partial}{\partial \bar{n}_{ij}} = \mp \frac{\partial}{\partial \bar{t}_{kj}}$ and $\frac{\partial}{\partial \bar{n}_{kj}} = \mp \frac{\partial}{\partial \bar{t}_{ij}}$.

The trace of a Powell-Sabin spline $s(x, y)$ along the boundary $\partial\Delta$ of a given triangulation Δ is a piecewise quadratic polynomial with specific continuity characteristics. It is globally C^1 -continuous, except at the case II boundary vertices. There, the spline is C^0 -continuous. A Powell-Sabin spline along the boundary can be described by a one-dimensional generalized (periodic) quadratic spline $\tilde{s}(w)$ in the classical B-spline representation [6],

$$\tilde{s}(w) = \sum_k \tilde{b}_k \tilde{N}_k(w), \quad (3.3)$$

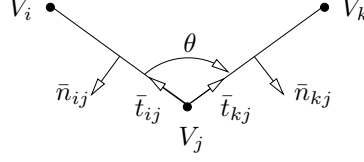


Figure 2: Orientation of the tangential directions (\bar{t}_{ij} and \bar{t}_{kj}), the normal directions (\bar{n}_{ij} and \bar{n}_{kj}), and the edge intersection angle θ at the boundary vertex V_j .

with w the accumulated arc length in counter-clockwise direction. As in [17], we associate the spline knots \tilde{t}_k with the positions of the vertices V_j and the points R_{ij} . The lengths of the knot intervals preserve the distances between the points R_{ij} and V_j . The notation and knot positions are illustrated in Figure 3(b). The support of a quadratic B-spline $\tilde{N}_k(w)$ is an interval spanned by four successive knots, starting with the knot \tilde{t}_k .

The normal derivative of a Powell-Sabin spline along $\partial\Delta$ is a piecewise linear polynomial, which we will represent by a one-dimensional generalized (periodic) linear spline $\hat{s}(w)$. As mentioned before, we chose the PS-refinement such that the interior line $Z-R_{ij}$ is normal to the boundary. Because of this choice, $\hat{s}(w)$ is linear on the edge V_i-V_j . This can be shown as follows. All points X on the line $Z-R_{ij}$ satisfy the equation

$$\bar{t}_{ij} \cdot (X - R_{ij}) = 0. \quad (3.4)$$

Consider a quadratic polynomial $p(x, y)$ on triangle $\rho(V_i, R_{ij}, Z)$ and another quadratic polynomial $q(x, y)$ on $\rho(R_{ij}, V_j, Z)$. The two patches are C^1 -continuous along the line $Z-R_{ij}$ if and only if

$$q(X) = p(X) + \lambda(\bar{t}_{ij} \cdot (X - R_{ij}))^2 \quad (3.5)$$

for some value of λ . Since the quadric $z(X) = (\bar{t}_{ij} \cdot (X - R_{ij}))^2$ is a parabolic cylinder with its axis parallel to \bar{n}_{ij} , it follows for all points in the combined triangle $\rho(V_i, V_j, Z)$ that

$$\frac{\partial z}{\partial \bar{n}_{ij}} = 0, \quad \text{and, hence,} \quad \frac{\partial q}{\partial \bar{n}_{ij}} = \frac{\partial p}{\partial \bar{n}_{ij}}. \quad (3.6)$$

Thus, the normal derivative of the Powell-Sabin spline is linear on the edge V_i-V_j . The 1D spline $\hat{s}(w)$ may be discontinuous at the point V_j in case II, and is C^0 -continuous in case I. Figure 3(c) shows the knot positions and some basis functions used to represent $\hat{s}(w)$. Because of the linearity along V_i-V_j , only knots at the boundary vertices are needed. The knots and coefficients of $\tilde{s}(w)$ and $\hat{s}(w)$ are distinguished by tildes and hats respectively.

We now derive a relation between the coefficients of $\tilde{s}(w)$ and $\hat{s}(w)$ at a case II boundary vertex V_j . Let $R_{ij} = \lambda_{ij}V_i + \lambda_{ji}V_j$ and $R_{jk} = \lambda_{jk}V_j + \lambda_{kj}V_k$ with $\lambda_{ij} + \lambda_{ji} = \lambda_{jk} + \lambda_{kj} = 1$. Then

$$\frac{\partial}{\partial \tilde{t}_{ij}} s(V_j) = -\tilde{s}'(\tilde{t}_{j_1}^-) = \frac{2}{\lambda_{ij}} \frac{(\tilde{b}_{i_2} - \tilde{b}_{ij})}{\|V_i - V_j\|}, \quad (3.7a)$$

$$\frac{\partial}{\partial \tilde{t}_{kj}} s(V_j) = \tilde{s}'(\tilde{t}_{j_1}^+) = \frac{2}{\lambda_{kj}} \frac{(\tilde{b}_{j_1} - \tilde{b}_{ij})}{\|V_k - V_j\|}. \quad (3.7b)$$

The normal derivatives of the Powell-Sabin spline at the vertex V_j are equal to

$$\frac{\partial}{\partial \bar{n}_{ij}} s(V_j) = \hat{s}(\hat{t}_{j_1}^-) = \hat{b}_{i_2}, \quad (3.8a)$$

$$\frac{\partial}{\partial \bar{n}_{kj}} s(V_j) = \hat{s}(\hat{t}_{j_1}^+) = \hat{b}_{j_1}. \quad (3.8b)$$

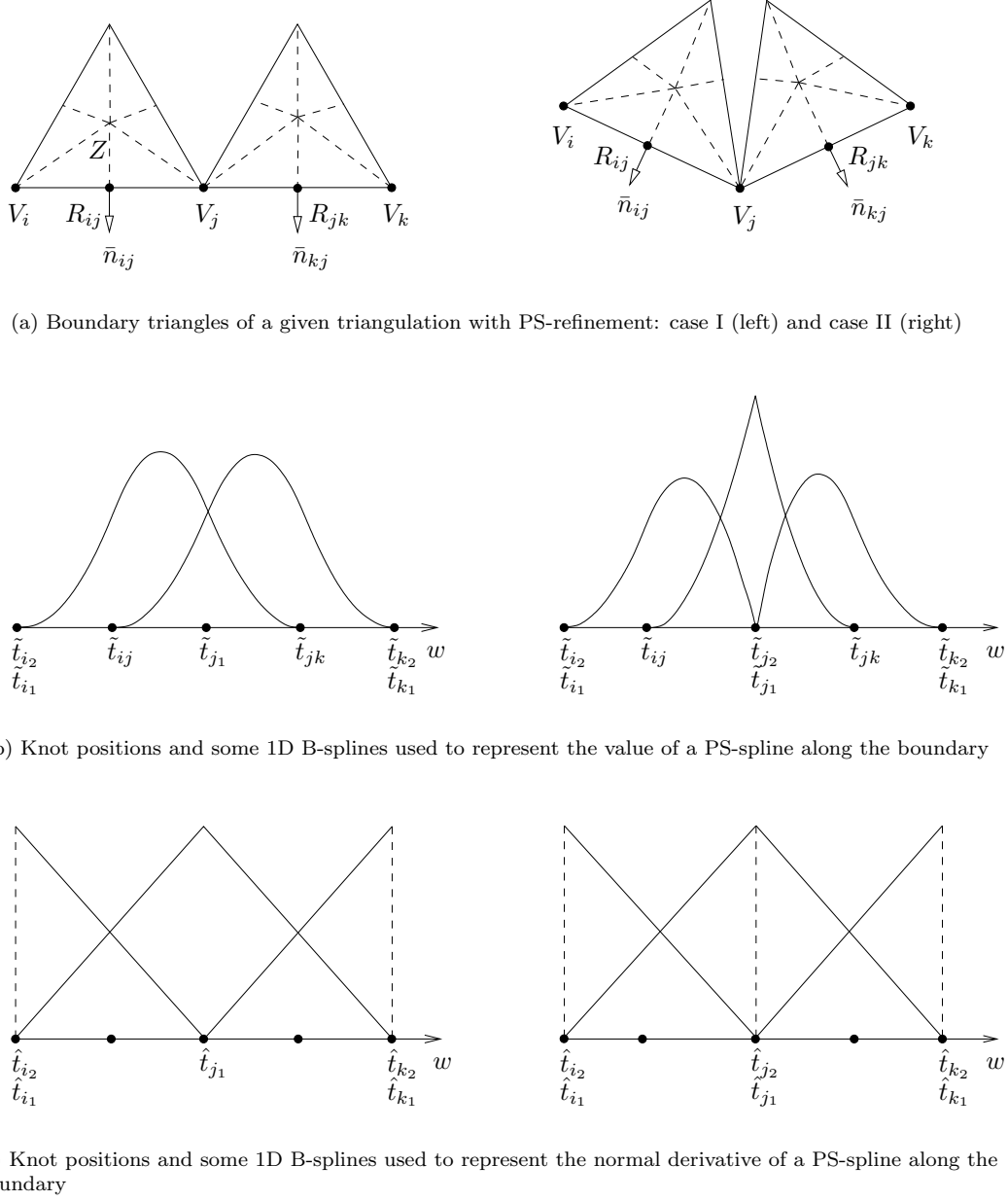


Figure 3: The knot positions and some 1D B-splines for the representation of (b) the value and (c) the normal derivative of a PS-spline along the boundary in case I and II.

Combining (3.7) and (3.8) with (3.2), we obtain a relation between the coefficients of the splines $\tilde{s}(w)$ and $\hat{s}(w)$:

$$\sin(\theta) \hat{b}_{i_2} = \frac{2 \cos(\theta)}{\lambda_{ij}} \frac{(\tilde{b}_{i_2} - \tilde{b}_{ij})}{\|V_i - V_j\|} - \frac{2}{\lambda_{kj}} \frac{(\tilde{b}_{j_1} - \tilde{b}_{ij})}{\|V_k - V_j\|}, \quad (3.9a)$$

$$\sin(\theta) \hat{b}_{j_1} = \frac{2 \cos(\theta)}{\lambda_{kj}} \frac{(\tilde{b}_{j_1} - \tilde{b}_{ij})}{\|V_k - V_j\|} - \frac{2}{\lambda_{ij}} \frac{(\tilde{b}_{i_2} - \tilde{b}_{ij})}{\|V_i - V_j\|}. \quad (3.9b)$$

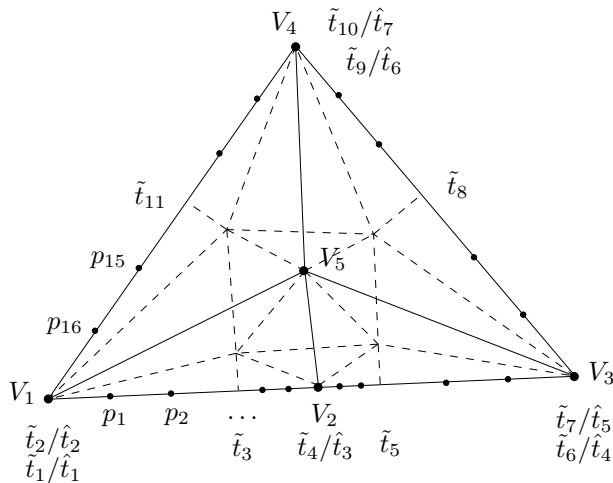


Figure 4: Example triangulation with knot positions for a Dirichlet (\tilde{t}_k) and Neumann (\hat{t}_k) boundary condition. Two sample points p_r are taken in each non-degenerated knot interval $[\tilde{t}_i, \tilde{t}_{i+1}]$.

For a case I boundary vertex ($\theta = \pi$) these relations reduce to

$$\frac{2}{\lambda_{kj}} \frac{(\tilde{b}_{j1} - \tilde{b}_{ij})}{\|V_k - V_j\|} + \frac{2}{\lambda_{ij}} \frac{(\tilde{b}_{i2} - \tilde{b}_{ij})}{\|V_i - V_j\|} = 0, \quad (3.10)$$

which is just the C^1 -continuity relation between the spline coefficients of $\tilde{s}(w)$ at V_j .

4 Boundary conditions on a polygonal boundary

We deal with the question of how to impose Dirichlet and Neumann boundary conditions on a Powell-Sabin spline. Physically, if that spline would represent, for example a temperature field, a Dirichlet condition corresponds to setting the value of the field variable, i.e. temperature. A Neumann condition specifies a flux condition on the boundary. We suppose that the boundary condition is defined on a polygonal domain boundary, so we can follow the approach proposed in [17], consisting of two steps. In a first step the boundary function is projected into the Powell-Sabin spline space. Representing the PS-spline with a one-dimensional generalized (periodic) spline defined along the boundary, a discrete least squares method [7] can be used to find a good approximation. In a second step the constraints on the PS-spline coefficients are determined such that the trace of the PS-spline along the boundary equals the projected boundary function. It turns out that a particular choice of the PS-triangles at the boundary can greatly simplify these constraints. We advocate an adaptation to the strategy in [17]: we will only use a single type of PS-triangles at the boundary.

To illustrate the projection into the PS-space of the functions appearing in the right hand sides of these boundary conditions, we will refer each time to the triangulation in Figure 4. It consists of a single case I boundary vertex (V_2), and three case II boundary vertices (V_1, V_3, V_4). The figure also shows corresponding knot positions of $\tilde{s}(w)$ and of $\hat{s}(w)$, starting with $\tilde{t}_1 = \hat{t}_1 = \tilde{t}_2 = \hat{t}_2 = 0$. The number of knots shown for each case is equal to the dimension of the corresponding 1D spline space. If we unfold the boundary of the triangulation to a straight line, we need to introduce some extra knots at both ends of the interval, e.g. $\tilde{t}_0, \tilde{t}_{12}$, and \tilde{t}_{13} to uniquely define $\tilde{s}(w) = \sum_{k=0}^{11} \tilde{b}_k \tilde{N}_k(w)$. These knots are chosen such that $\tilde{t}_{11} - \tilde{t}_0 = \tilde{t}_{12} = \tilde{t}_{13}$ equals the total boundary length, and $\tilde{b}_0 = \tilde{b}_{11}$

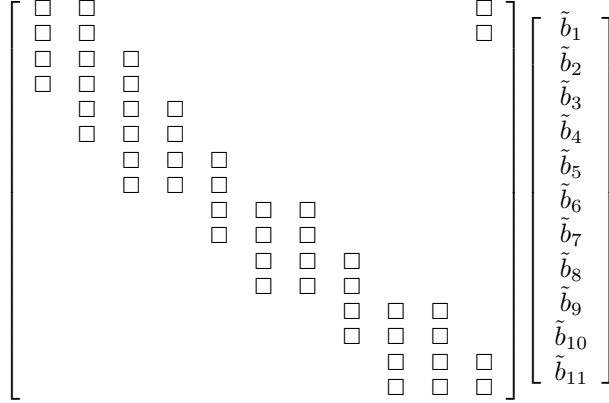


Figure 5: Band structure of the overdetermined system $\sum_k \tilde{b}_k \tilde{N}_k(w_r) = f(p_r)$ for a Dirichlet condition on the boundary of the triangulation in Figure 4. Two interpolation points p_r are chosen in each non-degenerated knot interval $[\tilde{t}_i, \tilde{t}_{i+1}]$.

to retain the periodicity of the spline. Likewise, $\hat{s}(w) = \sum_{k=1}^7 \hat{b}_k \hat{N}_k(w)$ with $\hat{t}_8 = \hat{t}_9$ equal to the boundary length.

4.1 A Dirichlet boundary condition

A Dirichlet condition on a Powell-Sabin spline $s(x, y)$ corresponds to the condition

$$s(x, y) = f(x, y), \quad \text{for } (x, y) \in \partial\Omega, \quad (4.1)$$

for a given function $f(x, y)$. A PS-spline cannot in general satisfy this condition exactly, unless the trace of $f(x, y)$ along $\partial\Omega$ is a one-dimensional quadratic spline satisfying the characteristics discussed in section 3. If this is not the case, we shall first project the function f into the appropriate spline space. Here, we suggest to use the approximation $\tilde{s}(w)$ obtained by a discrete least squares method. We take a number of evaluation points p_r along the boundary (in the example of Figure 4 two points in each knot interval), calculate the corresponding values w_r for the accumulated arc length, and determine the coefficients \tilde{b}_k as the least squares solution of the overdetermined system $\sum_k \tilde{b}_k \tilde{N}_k(w_r) = f(p_r)$. Here, we can fully exploit the typical cyclic bandstructure as shown in Figure 5 for the triangulation in Figure 4.

Once the coefficients \tilde{b}_k are known, one can proceed to derive the constraints on the PS-spline coefficients $c_{i,j}$ in (2.3) such that the Powell-Sabin spline exactly matches $\tilde{s}(w)$ at the boundary. The construction of those constraints is explained below. It is sufficient to impose the following three conditions for each vertex V_j (see [17])

$$s(V_j) = \tilde{s}(\tilde{t}_{j_1}), \quad \frac{\partial}{\partial \tilde{t}_{ij}} s(V_j) = -\tilde{s}'(\tilde{t}_{j_1} -), \quad \text{and} \quad \frac{\partial}{\partial \tilde{t}_{kj}} s(V_j) = \tilde{s}'(\tilde{t}_{j_1} +). \quad (4.2)$$

We choose the PS-triangle of V_j such that one side is parallel to the boundary edge V_i - V_j , and another side of the PS-triangle is normal to that edge. Let τ_{ij} and ν_{ij} be such that

$$Q_{j,2} - Q_{j,1} = \tau_{ij} \tilde{t}_{ij}, \quad \text{and} \quad Q_{j,3} - Q_{j,1} = \nu_{ij} \bar{n}_{ij}. \quad (4.3)$$

One can always find such constrained PS-triangles with a reasonable small area. They can be constructed as follows. The radius r of the inscribed circle of a triangle is equal to

$$r = \frac{2A}{l_1 + l_2 + l_3}, \quad (4.4)$$

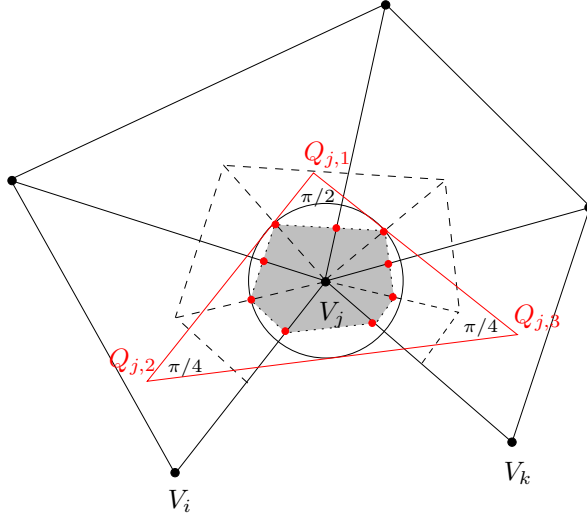


Figure 6: PS-triangle of vertex V_j , such that the inscribed circle contains all PS-points. The triangle is right-angled and isosceles. The convex hull of the PS-points is shaded.

with A the area of the triangle, and l_i the lengths of the sides. We choose the PS-triangle of boundary vertex V_j to be isosceles, with the right angle as its top, as shown in Figure 6. Using this property together with (4.4), the area of the resulting PS-triangle can be written as

$$A = r^2(2\sqrt{2} + 3). \quad (4.5)$$

Let the centre of the inscribed circle coincide with vertex V_j . Then, the circle contains all PS-points if the radius r is larger than half the longest of the considered edges. Thus, with h_{\max}^* the length of the longest edge in the PS-refinement, the area of the PS-triangles is bounded by

$$A \leq h_{\max}^{*2}(2\sqrt{2} + 3)/4 \simeq 1.46 h_{\max}^{*2}. \quad (4.6)$$

Since the hypotenuse is the longest side in a right triangle, and in our case $A = l^2/4$ with l the length of the hypotenuse, the lengths of the sides of the PS-triangles can be bounded by

$$l_i \leq l \leq h_{\max}^* \sqrt{2\sqrt{2} + 3} \simeq 2.41 h_{\max}^*. \quad (4.7)$$

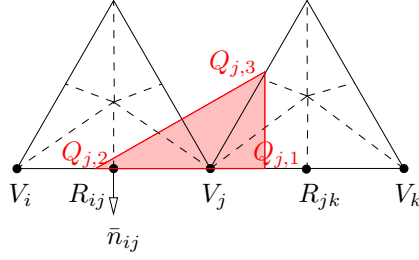
It is possible to construct other PS-triangles, satisfying (4.3), that have a smaller area. Figure 7 shows such PS-triangles for different boundary situations.

Using the tangent property of the PS-control triangle and the constraint (4.3), the derivatives of the Powell-Sabin spline at V_j in the directions \bar{t}_{ij} and \bar{n}_{ij} are proportional to $c_{j,2} - c_{j,1}$ and $c_{j,3} - c_{j,1}$. Together with relation (3.2a), it follows that

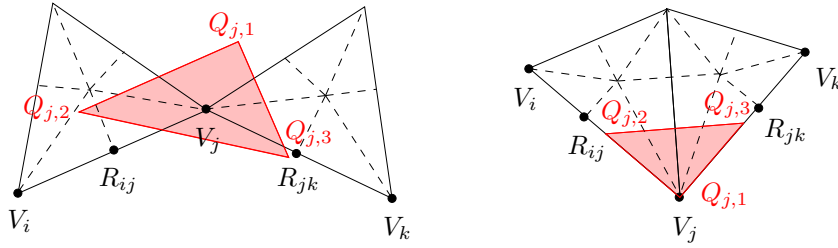
$$s(V_j) = \sum_{l=1}^3 \alpha_{j,l} c_{j,l}, \quad (4.8a)$$

$$\frac{\partial}{\partial \bar{t}_{ij}} s(V_j) = \frac{c_{j,2} - c_{j,1}}{\tau_{ij}}, \quad (4.8b)$$

$$\frac{\partial}{\partial \bar{t}_{kj}} s(V_j) = \cos(\theta) \frac{c_{j,2} - c_{j,1}}{\tau_{ij}} - \sin(\theta) \frac{c_{j,3} - c_{j,1}}{\nu_{ij}}. \quad (4.8c)$$



(a) Case I boundary



(b) Case II boundary

Figure 7: Choice of the PS-triangles, constrained with one side parallel and another side normal to the edge V_i-V_j , at a boundary in case I and II.

Substituting (4.8) into (4.2), using the fact that $\alpha_{j,1} + \alpha_{j,2} + \alpha_{j,3} = 1$, and after rearranging terms, we obtain the constraints

$$c_{j,1} + \alpha_{j,2}(c_{j,2} - c_{j,1}) + \alpha_{j,3}(c_{j,3} - c_{j,1}) = \tilde{b}_{ij}, \quad (4.9a)$$

$$c_{j,2} - c_{j,1} = \frac{2\tau_{ij}(\tilde{b}_{i2} - \tilde{b}_{ij})}{\lambda_{ij} \|V_i - V_j\|}, \quad (4.9b)$$

$$\sin(\theta)(c_{j,3} - c_{j,1}) = 2\nu_{ij} \left(\cos(\theta) \frac{1}{\lambda_{ij}} \frac{(\tilde{b}_{i2} - \tilde{b}_{ij})}{\|V_i - V_j\|} - \frac{1}{\lambda_{kj}} \frac{(\tilde{b}_{j1} - \tilde{b}_{ij})}{\|V_k - V_j\|} \right). \quad (4.9c)$$

Remark 4.1. These constraints can be simplified in some particular situations. If the domain makes an acute angle (less than $\pi/2$) at vertex V_j , we can choose $Q_{j,1} = V_j$. Since the triplet $(\alpha_{j,1}, \alpha_{j,2}, \alpha_{j,3})$ is the barycentric coordinate of V_j with respect to the PS-triangle, it follows that $\alpha_{j,2} = \alpha_{j,3} = 0$, and constraint (4.9a) simplifies then to $c_{j,1} = \tilde{b}_{ij}$. In the case $\theta = \pi/2$, as shown in the right panel of Figure 7(b), the PS-triangle has two sides parallel to the boundary. The constraints (4.9) simplify then to

$$c_{j,1} = \tilde{b}_{ij}, \quad (4.10a)$$

$$c_{j,2} = \tilde{b}_{ij} + \frac{2\tau_{ij}(\tilde{b}_{i2} - \tilde{b}_{ij})}{\lambda_{ij} \|V_i - V_j\|}, \quad (4.10b)$$

$$c_{j,3} = \tilde{b}_{ij} - \frac{2\nu_{ij}(\tilde{b}_{j1} - \tilde{b}_{ij})}{\lambda_{kj} \|V_k - V_j\|}. \quad (4.10c)$$

Remark 4.2. A case I boundary can be considered as a limit case of the case II situation. Since the left-hand side of equation (4.9c) becomes zero, the constraint reduces to the C^1 -continuity relation (3.10). Hence, only the constraints (4.9a) and (4.9b) on the Powell-Sabin spline coefficients remain.

Remark 4.3. For the case I boundary, it is possible to let one side of the PS-triangle coincide with the boundary line, i.e. $V_j = \alpha_{j,1}Q_{j,1} + \alpha_{j,2}Q_{j,2}$. This type of PS-triangle is depicted in Figure 7(a). With this particular choice, the Powell-Sabin B-spline $B_j^3(x, y)$ vanishes at the domain boundary, and the value of the corresponding coefficient $c_{j,3}$ will not be constrained by the Dirichlet boundary condition. Setting $\alpha_{j,3}$ equal to zero, we arrive at the conditions

$$c_{j,1} = \tilde{b}_{ij} - \alpha_{j,2} \frac{2\tau_{ij}}{\lambda_{ij}} \frac{(\tilde{b}_{i_2} - \tilde{b}_{ij})}{\|V_i - V_j\|}, \quad (4.11a)$$

$$c_{j,2} = \tilde{b}_{ij} + \alpha_{j,1} \frac{2\tau_{ij}}{\lambda_{ij}} \frac{(\tilde{b}_{i_2} - \tilde{b}_{ij})}{\|V_i - V_j\|}. \quad (4.11b)$$

Taking into account that the 1D spline $\tilde{s}(w)$ is C^1 -continuous at V_j , i.e. with a single knot at V_j and using the 1D B-splines in the left panel of Figure 3(b), we obtain the constraints from [17]:

$$c_{j,1} = \tilde{b}_{i_2} + \delta \left(1 + \frac{2\tau_{ij} \alpha_{j,2}}{\lambda_{ij} \|V_i - V_j\|} \right) (\tilde{b}_{ij} - \tilde{b}_{i_2}), \quad (4.12a)$$

$$c_{j,2} = \tilde{b}_{i_2} + \delta \left(1 - \frac{2\tau_{ij} \alpha_{j,1}}{\lambda_{ij} \|V_i - V_j\|} \right) (\tilde{b}_{ij} - \tilde{b}_{i_2}), \quad (4.12b)$$

with

$$\delta = \frac{\tilde{t}_{j_1} - \tilde{t}_{ij}}{\tilde{t}_{jk} - \tilde{t}_{ij}}.$$

Remark 4.4. For a case II boundary, the PS-triangle is proposed in [17] to have two sides parallel to the boundary edges. This leads to constraints that are similar to (4.10), and are simpler than (4.9). Yet, when the boundary angle θ is sufficiently close to π , this construction results in a PS-triangle that becomes increasingly large, leading to a poorly conditioned Powell-Sabin B-spline basis. Our choice of PS-triangle with (4.3) stays stable, regardless of the boundary angle.

4.2 A Neumann boundary condition

A Neumann condition implies that the outward normal derivative of the Powell-Sabin spline is specified on the boundary, i.e.,

$$\frac{\partial}{\partial \bar{n}} s(x, y) = g(x, y), \quad \text{for } (x, y) \in \partial\Omega. \quad (4.13)$$

Similar to the Dirichlet case, a PS-spline will generally not be able to satisfy the boundary condition exactly, unless the trace of $g(x, y)$ happens to belong to the appropriate 1D spline space. We may need to approximate $g(x, y)$ along the boundary by the one-dimensional linear spline $\hat{s}(w)$, using e.g. discrete least squares. The typical band structure of the overdetermined system $\sum_k \hat{b}_k \hat{N}_k(w_r) = g(p_r)$ is illustrated in Figure 8.

We use a PS-triangle with one side parallel to edge $V_i - V_j$ and another side orthogonal to that edge, as in the Dirichlet case. Using the tangent property of the PS-triangle and (3.2b), we arrive at

$$\frac{\partial}{\partial \bar{n}_{ij}} s(V_j) = \frac{c_{j,3} - c_{j,1}}{\nu_{ij}}, \quad (4.14a)$$

$$\frac{\partial}{\partial \bar{n}_{kj}} s(V_j) = -\sin(\theta) \frac{c_{j,2} - c_{j,1}}{\tau_{ij}} - \cos(\theta) \frac{c_{j,3} - c_{j,1}}{\nu_{ij}}. \quad (4.14b)$$

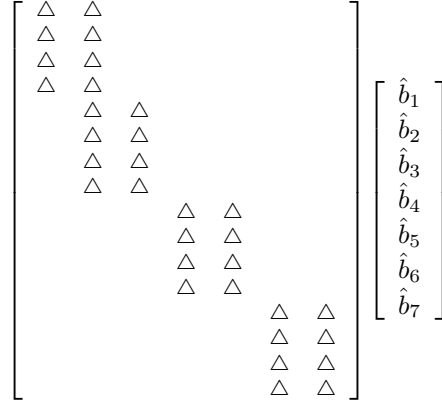


Figure 8: Band structure of the overdetermined system $\sum_k \hat{b}_k \hat{N}_k(w_r) = g(p_r)$ for a Neumann condition on the boundary of the triangulation in Figure 4. Four interpolation points p_r are chosen in each non-degenerated knot interval $[\hat{t}_l, \hat{t}_{l+1}]$.

The Neumann constraints on the Powell-Sabin spline coefficients are obtained by imposing the conditions (3.8) for each vertex V_j . The constraints (4.14) can then be written as

$$c_{j,3} - c_{j,1} = \nu_{ij} \hat{b}_{i_2}, \quad (4.15a)$$

$$\sin(\theta) (c_{j,2} - c_{j,1}) = -\tau_{ij} (\hat{b}_{j_1} + \cos(\theta) \hat{b}_{i_2}). \quad (4.15b)$$

Remark 4.5. For a case I boundary vertex, the constraint (4.15b) can be omitted. It leads to the condition $\hat{b}_{j_1} = \hat{b}_{i_2}$, which corresponds to the requirement of continuity.

Remark 4.6. In [17] a PS-triangle with two sides normal to the boundary edges is proposed, which results in two constraints similar to (4.15a), but their use requires a treatment for the Neumann condition that is different from that of the Dirichlet condition.

Remark 4.7. Unlike a Dirichlet condition, a Neumann condition does not uniquely define the trace of a function at the boundary. The Powell-Sabin spline constraints (4.15) reflect this property, as they only impose a condition on the *difference* of two coefficients.

4.3 Combination of Dirichlet and Neumann boundary condition

The type of boundary conditions may change on different parts of the domain boundary. In order to illustrate how such a situation can be handled, we consider an example. Suppose that the boundary vertex V_j of the triangulation is a point where a Dirichlet condition along edge V_i-V_j meets a Neumann condition along edge V_j-V_k . As motivated before, we will use the same type of PS-triangles for the Dirichlet and Neumann sections. Of course, the 1D splines $\tilde{s}(w)$ and $\hat{s}(w)$ are only meaningful on the relevant parts of the boundary.

To obtain the relations between the 1D spline coefficients and the Powell-Sabin spline coefficients, we impose the conditions

$$s(V_j) = \tilde{s}(\tilde{t}_{j_1}), \quad \frac{\partial}{\partial \tilde{t}_{ij}} s(V_j) = -\tilde{s}'(\tilde{t}_{j_1} -), \quad \text{and} \quad \frac{\partial}{\partial \tilde{n}_{kj}} s(V_j) = \hat{s}(\hat{t}_{j_1} +). \quad (4.16)$$

Using equations (4.8a), (4.8b) and (4.14b), one finds that (4.16) is equivalent to the constraints

$$c_{j,1} + \alpha_{j,2} (c_{j,2} - c_{j,1}) + \alpha_{j,3} (c_{j,3} - c_{j,1}) = \tilde{b}_{ij}, \quad (4.17a)$$

$$c_{j,2} - c_{j,1} = \frac{2\tau_{ij} (\tilde{b}_{i_2} - \tilde{b}_{ij})}{\lambda_{ij} \|V_i - V_j\|}, \quad (4.17b)$$

$$\cos(\theta) (c_{j,3} - c_{j,1}) = -\nu_{ij} \left(\hat{b}_{j_1} + \sin(\theta) \frac{2 (\tilde{b}_{i_2} - \tilde{b}_{ij})}{\lambda_{ij} \|V_i - V_j\|} \right). \quad (4.17c)$$

Remark 4.8. When the two boundary edges are orthogonal to each other, the third constraint (4.17c) becomes redundant and can be omitted, since

$$\hat{b}_{j_1} = -\sin(\theta) \frac{2 (\tilde{b}_{i_2} - \tilde{b}_{ij})}{\lambda_{ij} \|V_i - V_j\|}, \quad (4.18)$$

in accordance with relation (3.9b). For $\theta = \pi/2$, the reduced set of constraints simplifies to

$$c_{j,1} = \tilde{b}_{ij}, \quad (4.19a)$$

$$c_{j,2} = \tilde{b}_{ij} + \frac{2\tau_{ij} (\tilde{b}_{i_2} - \tilde{b}_{ij})}{\lambda_{ij} \|V_i - V_j\|}, \quad (4.19b)$$

when we choose $Q_{j,1} = V_j$, referring to Remark 4.1.

Other types of boundary conditions that combine Dirichlet and Neumann conditions, can be treated in a similar fashion. For example, a Cauchy boundary condition which specifies both the value (4.1) and the normal slope (4.13) at the boundary. Here, we determine the coefficients of both splines $\tilde{s}(w)$ and $\hat{s}(w)$. During the computation of the 1D spline coefficients, we have to enforce the relations (3.9), corresponding to the behaviour of a PS-spline. In the projection step, we now solve the following constrained minimization problem,

$$\min \omega_D \sum_{r=1}^m (f(p_r) - \tilde{s}(w_r))^2 + \omega_N \sum_{r=1}^m (g(p_r) - \hat{s}(w_r))^2, \quad \text{subject to (3.9)}, \quad (4.20)$$

for some weights ω_D and ω_N . A Cauchy boundary conditions is sometimes called a weighted average of imposing a Dirichlet and a Neumann condition. The term refers to an average that takes into account the proportional relevance of each component, dependent on which information is available for the well-posedness of the problem and its subsequent successful solution. The corresponding set of constraints on the PS-spline coefficients is formed by (4.9a), (4.9b) and (4.15a) for each boundary vertex V_j . Hence, the values of all coefficients associated to a boundary vertex will be determined.

5 Boundary conditions on curved domains

This section addresses Powell-Sabin splines with boundary conditions defined on a curved domain boundary $\partial\Omega^c$. Such a domain boundary cannot be exactly represented by a triangulation. We suppose that the boundary vertices of the triangulation are located on the curved line.

5.1 A Dirichlet boundary condition

We try to impose a Dirichlet boundary condition on a Powell-Sabin spline, i.e. (4.1), where the function $f(x, y)$ is given on a curved domain boundary $\partial\Omega^c$. This introduces two kinds of errors:

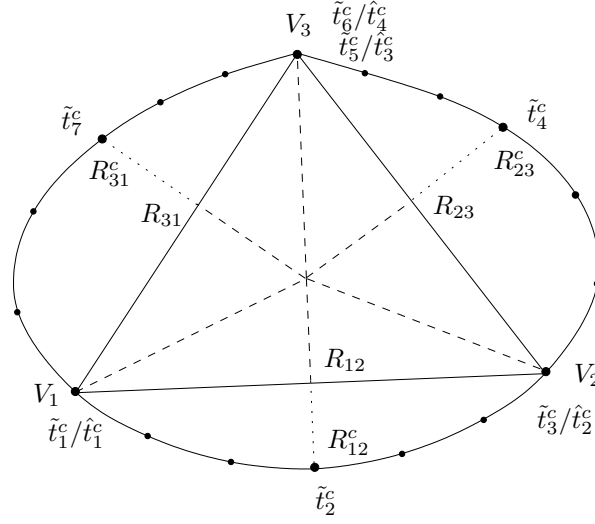


Figure 9: Example triangulation with knot positions for a Dirichlet (\tilde{t}_k^c) and Neumann (\hat{t}_k^c) boundary condition, defined on a curved domain boundary.

errors caused by the quadratic nature of the spline, and errors caused by the linear approximation of the domain boundary. Contrary to the polygonal case in section 4, the PS-spline is not always defined along the boundary of the physical domain, i.e., when the boundary curve lies outside the triangulation. In addition, if the curve is inside, the behaviour of the Powell-Sabin spline along the trace of the curve depends on the type of the curve. For instance, the spline behaves as a piecewise quadratic polynomial along a linear line, and as a piecewise quartic polynomial along a parabolic curve. As in the polygonal case we distinguish two boundary situations: a smooth curve, i.e. C^1 -continuous, at vertex V_j (case I^c), and a curve with a tangential discontinuity at V_j (case II^c). The triangulation in Figure 9 consists of two case I^c boundary vertices (V_1, V_2), and a single case II^c boundary vertex (V_3).

Our approach is to approximate in a first step the trace of $f(x, y)$ along $\partial\Omega^c$ by a 1D quadratic spline $\tilde{s}(w^c)$, e.g. with a discrete least squares method. Here, w^c is the accumulated arc length in counter-clockwise direction along the boundary curve. The spline knots of $\tilde{s}(w^c)$ are assigned to the vertices V_j and the interjacent points R_{ij}^c at the boundary curve, as illustrated in Figure 9. Single knots, denoted as \tilde{t}_{ij}^c , are associated with the points R_{ij}^c . Double knots, i.e. $\tilde{t}_{j_1}^c$ and $\tilde{t}_{j_2}^c$, are assigned to the case II^c boundary vertices V_j ; a single knot $\tilde{t}_{j_1}^c$ is assigned to V_j otherwise. We select the lengths of the knot intervals so that they preserve the boundary curve arc lengths between the points R_{ij}^c and V_j .

In a second step, we compose a set of constraints on the PS-spline coefficients such that the PS-spline will approximately match $\tilde{s}(w^c)$. At the points V_j , we impose that the value and tangential derivatives of the Powell-Sabin spline are equal to the value and tangential derivatives of $\tilde{s}(w^c)$ at these points. I.e., we impose the conditions (4.2) where \bar{t}_{ij} and \bar{t}_{kj} are the directions tangent to the boundary curve at V_j in clockwise and counter-clockwise direction. If the boundary curve is polygonal, these conditions ensure that $\tilde{s}(w^c)$ exactly matches the trace of the Powell-Sabin spline along the boundary.

In order to simplify the constraints, we suggest to use a PS-triangle with one side parallel to \bar{t}_{ij} , and another side orthogonal to \bar{t}_{ij} , as illustrated in Figure 10. We obtain then a set of constraints

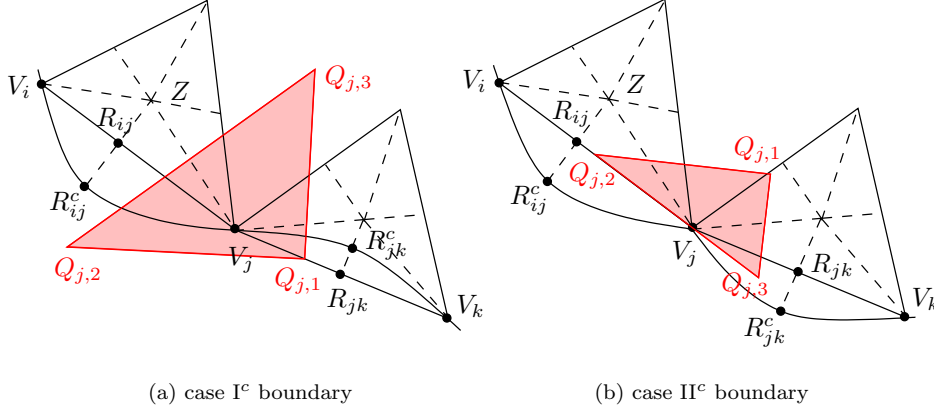


Figure 10: Choice of the boundary PS-triangles in case of a curved boundary.

on the PS-spline coefficients, analogous to the ones in the polygonal case (4.9):

$$c_{j,1} + \alpha_{j,2} (c_{j,2} - c_{j,1}) + \alpha_{j,3} (c_{j,3} - c_{j,1}) = \tilde{b}_{ij}, \quad (5.1a)$$

$$c_{j,2} - c_{j,1} = 2\tau_{ij} \frac{\tilde{b}_{i2} - \tilde{b}_{ij}}{\tilde{t}_{j1}^c - \tilde{t}_{ij}^c}, \quad (5.1b)$$

$$\sin(\theta) (c_{j,3} - c_{j,1}) = 2\nu_{ij} \left(\cos(\theta) \frac{\tilde{b}_{i2} - \tilde{b}_{ij}}{\tilde{t}_{j1}^c - \tilde{t}_{ij}^c} - \frac{\tilde{b}_{j1} - \tilde{b}_{ij}}{\tilde{t}_{jk}^c - \tilde{t}_{j1}^c} \right), \quad (5.1c)$$

where θ stands for the angle between the tangential vectors \bar{t}_{ij} and \bar{t}_{kj} at V_j .

Remark 5.1. For a smooth boundary curve (case I^c) with $\theta = \pi$, the constraint (5.1c) can be omitted, since it reduces to the C^1 -continuity relation between the 1D B-spline coefficients at \tilde{t}_{j1}^c .

Remark 5.2. When the boundary function $f(x, y)$ of the Dirichlet condition (4.1) is smooth, one can approximate the condition, alternatively, by a direct Hermite interpolation, i.e.,

$$c_{j,1} + \alpha_{j,2} (c_{j,2} - c_{j,1}) + \alpha_{j,3} (c_{j,3} - c_{j,1}) = f(V_j), \quad (5.2a)$$

$$c_{j,2} - c_{j,1} = \tau_{ij} \frac{\partial}{\partial \tilde{t}_{ij}} f(V_j), \quad (5.2b)$$

$$\sin(\theta) (c_{j,3} - c_{j,1}) = \nu_{ij} \left(\cos(\theta) \frac{\partial}{\partial \tilde{t}_{ij}} f(V_j) - \frac{\partial}{\partial \tilde{t}_{kj}} f(V_j) \right). \quad (5.2c)$$

5.2 A Neumann boundary condition

Similar to the polygonal case, we first approximate the trace of the function $g(x, y)$ of the Neumann condition along the curved boundary by a one-dimensional linear spline $\hat{s}(w^c)$. The knots \hat{t}_k^c are assigned to the vertices V_j , as illustrated in Figure 9. The set of constraints on the PS-spline coefficients are obtained by imposing at these vertices the conditions (3.8). The directions \bar{n}_{ij} and \bar{n}_{kj} are the left and right normal directions to the curve at V_j . If we consider the PS-triangles with one side tangent and another normal to the boundary curve, as in Figure 10, we can use for each boundary vertex V_j the same set of constraints as in the polygonal case, i.e. (4.15).

Remark 5.3. For a case I^c boundary curve, one of the constraints (4.15) can be omitted, since it reduces to the continuity relation between the B-spline coefficients at \hat{t}_{j1}^c .

6 Numerical examples

We consider the Poisson equation

$$-\Delta u = f, \quad \text{in } \Omega \in \mathbb{R}^2, \quad (6.1a)$$

with Ω the unit disk, and subject to Dirichlet and Neumann conditions on the boundary segments $\partial\Omega_D = \partial\Omega|_{x \leq 0}$ and $\partial\Omega_N = \partial\Omega|_{x > 0}$ respectively,

$$u = g_D \quad \text{on } \partial\Omega_D, \quad \text{and} \quad \frac{\partial u}{\partial \bar{n}} = g_N \quad \text{on } \partial\Omega_N. \quad (6.1b)$$

The functions f , g_D and g_N are chosen such that the solution is $u(x, y) = x^4 (x-1)^2 y^4 (y-1)^2$. We will construct a Powell-Sabin spline approximation $s(x, y)$ of the form (2.3) by using the standard Galerkin approach for the discretisation of the Poisson equation. In [17], an analytical formulation for the elements of the stiffness matrix is derived. We will solve the problem on successively refined triangulations. The initial mesh consists of six equilateral triangles; the other meshes are obtained by a $\sqrt{3}$ -refinement [16]. A special treatment is needed at the boundary to ensure the refined triangulation approximates the circular domain more accurately. In Figure 11 such a triangulation, after three refinement steps, is shown together with three different choices of the PS-triangles at the boundary to meet the treatment of the boundary condition. Figure 11(a) follows the approach of [17], where the sides of the PS-triangle coincide with the boundary edges. It is easy to see that after a few refinements, such PS-triangles become unacceptably narrow, which leads to poorly conditioned basis functions near the domain boundary. In Figure 11(b) we show PS-triangles which are constrained by (4.3). If we take into account that the physical domain is circular, we can choose one side tangential and another side normal to the boundary curve, as proposed in §5.1. This is shown in Figure 11(c).

Firstly, we solve problem (6.1), where the boundary condition is imposed on the boundary of the triangulation, such that we can apply constraints (4.9) and (4.15). Figure 12 shows the reduction of the error, measured by

$$\frac{\|u(x, y) - s(x, y)\|_{L_2(\Delta)}}{\text{area}(\Delta)}. \quad (6.2)$$

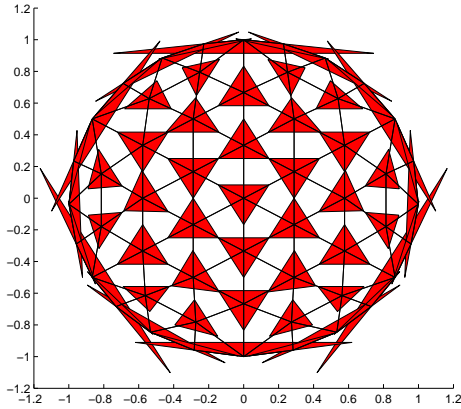
Since the successive triangulations have a different area, a fair comparison requires us to use an L_2 -norm scaled by the area of the triangulation. The error converges as $\mathcal{O}(h_{\max}^3)$.

We now solve the Poisson equation (6.1) with the boundary condition imposed on the boundary of the unit disk. We will treat the boundary condition in two different ways. First, we map condition (6.1b) to a similar type of condition on the boundary of the triangulation. More precisely, we impose that the PDE solution equals $g_{D,\Delta}$ on $\partial\Delta_D = \partial\Delta|_{x \leq 0}$ and the normal derivative equals $g_{N,\Delta}$ on the remaining part of the boundary of the triangulation, where $g_{D,\Delta}$ and $g_{N,\Delta}$ are obtained by mapping points on the polygonal boundary to points on the circle:

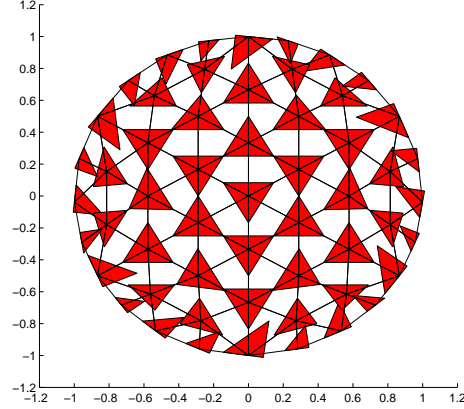
$$g_{D,\Delta}(X_D) = g_D(Y_D), \quad \text{with } X_D \in \partial\Delta_D, \quad \text{and } Y_D = \arg \min_{Z \in \partial\Omega_D} \|X_D - Z\|,$$

$$g_{N,\Delta}(X_N) = g_N(Y_N), \quad \text{with } X_N \in \partial\Delta_N, \quad \text{and } Y_N = \arg \min_{Z \in \partial\Omega_N} \|X_N - Z\|.$$

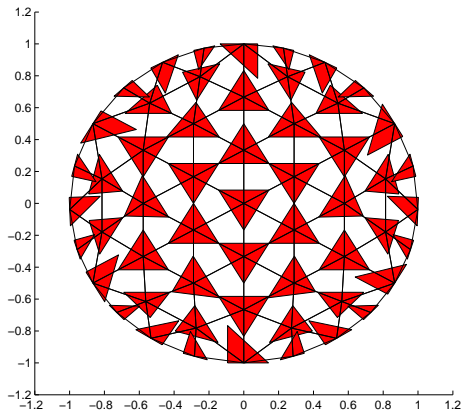
Then the method of §4 can be applied. It is similar to the robust approach in [1]. Secondly, we apply the curved constraints as proposed in §5. Both sets of boundary constraints can be easily eliminated from the Galerkin discretised linear system. We expect that the latter method is better. In the polygonal case, the trace along the boundary is C^1 -discontinuous at the vertices, meaning that for each boundary vertex three Dirichlet constraints or two Neumann constraints are imposed. The real (circular) boundary curve is, however, C^1 -continuous. Thus, the second method requires only two Dirichlet constraints or one Neumann constraint for each vertex, leaving more degrees



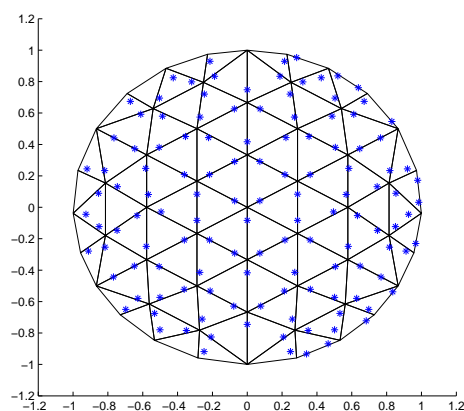
(a) Choice of the PS-triangles in case of a polygonal boundary, following the approach of [17].



(b) Choice of the PS-triangles in case of a polygonal boundary, as proposed in §4.



(c) Choice of the PS-triangles in case of a circular boundary, as in §5.



(d) Choice of the collocation points, based on the positions of the maxima of the PS B-splines.

Figure 11: Choice of PS-triangles in case of (a)-(b) a polygonal boundary, and (c) a curved boundary. (d) Possible placement of the collocation points for the mesh and the PS-triangles in (c), based on the positions of the maxima of the Powell-Sabin B-splines..

of freedom to satisfy (6.1). Figure 12 shows the reduction of the error for both approaches. The second approach leads to a more accurate solution, with the expected order of convergence.

In a Galerkin finite element approach for solving differential equations, a Neumann condition does not strictly need to be enforced on the elements of the approximation space. As natural boundary conditions, they are usually satisfied automatically. Enforcing a Neumann condition explicitly on the elements of the approximation space is nevertheless useful in, e.g., collocation methods. The collocation method has several advantages to the Galerkin method: no expensive scalar products

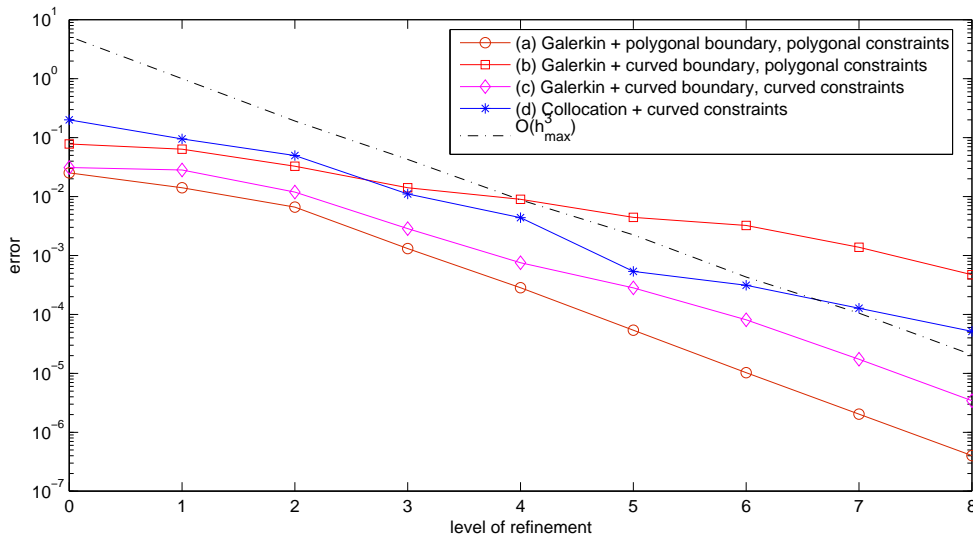


Figure 12: Using successively $\sqrt{3}$ -refined meshes approximating a unit disk, as in Figure 11, the norm of the error (6.2) for PDE (6.1) is showed in case the boundary condition is treated on the boundary of the triangulation (a), compared with three treatments on the real (curved) boundary (b)-(d). The Galerkin (a)-(c) and collocation (d) discretisation is considered.

have to be calculated, and the system of equations is a lot more sparse. To ensure the existence of a solution, there must lie at least three collocation points in the molecule of each vertex, except at the boundary vertices where the number depends on the kind of boundary condition. To satisfy the above requirement, one can place the collocation points at the positions of the maxima of the normalized Powell-Sabin B-splines, as illustrated in Figure 11(d). Figure 12 shows the reduction of the error for the collocation method applied to (6.1). Despite the advantages, spline collocation methods are not extensively used. An optimal placement of the collocation points is not trivial, and is only derived for certain degree splines on rectangular grid discretisations [2].

7 Concluding remarks

In this paper we addressed the question of how to impose boundary conditions on Powell-Sabin splines. We showed that imposing boundary conditions leads to sets of simple constraints on the PS-spline coefficients. We discussed Dirichlet and Neumann boundary conditions, defined on polygonal and non-polygonal domains. The general principle is twofold: first we project the boundary function to a one-dimensional spline space, and then the constraints on the PS-spline coefficients are determined.

A careful choice of the PS-triangles at the boundary can simplify the boundary constraints. We advocate a PS-triangle with one side tangential and another normal to the boundary curve. Other particular choices, as proposed in [17], can lead to some simpler constraints. Yet, our type of boundary PS-triangle has the advantage that the corresponding basis functions are always well conditioned, also when the boundary edges of the triangulation have an angle close to π . In addition, since we use the same type of PS-triangles regardless of the type of boundary condition, we can construct the basis in advance, irrespective of the particular application.

Acknowledgement

Hendrik Speleers is funded as a Research Assistant of the Fund for Scientific Research Flanders (Belgium).

References

- [1] J.H. Bramble and J.T. King. A robust finite element method for non-homogeneous Dirichlet problems in domains with curved boundaries. *Math. Comput.*, 63(207):1–17, 1994.
- [2] C.C. Christara. Quadratic spline collocation methods for elliptic partial differential equations. *BIT*, 34(1):33–61, 1994.
- [3] C.K. Chui and L.L. Schumaker. On spaces of piecewise polynomials with boundary conditions I. Rectangles. In W. Schempp and K. Zeller, editors, *Multivariate Approx. Theory II*, pages 69–80, Basel, 1982. Birkhäuser.
- [4] C.K. Chui, L.L. Schumaker, and R.H. Wang. On spaces of piecewise polynomials with boundary conditions II. Type-1 triangulations. In Z. Ditzian, A. Meir, S. Riemenschneider, and A. Sharma, editors, *Second Edmonton Conf. on Approx. Theory*, pages 51–66, Providence, 1983. AMS.
- [5] C.K. Chui, L.L. Schumaker, and R.H. Wang. On spaces of piecewise polynomials with boundary conditions III. Type-2 triangulations. In Z. Ditzian, A. Meir, S. Riemenschneider, and A. Sharma, editors, *Second Edmonton Conf. on Approx. Theory*, pages 67–80, Providence, 1983. AMS.
- [6] C. de Boor. On calculating with B-splines. *J. Approx. Theory*, 6:50–62, 1972.
- [7] P. Dierckx. *Curve and Surface Fitting with Splines*. Oxford University Press, Oxford, 1993.
- [8] P. Dierckx. On calculating normalized Powell-Sabin B-splines. *Comput. Aided Geom. Design*, 15(3):61–78, 1997.
- [9] P. Dierckx, S. Van Leemput, and T. Vermeire. Algorithms for surface fitting using Powell-Sabin splines. *IMA J. Numer. Anal.*, 12:271–299, 1992.
- [10] K. Höllig, U. Reif, and J. Wipper. Weighted extended B-spline approximation of Dirichlet problems. *SIAM J. Numer. Anal.*, 39(2):442–462, 2001.
- [11] C. Manni and P. Sablonnière. Quadratic spline quasi-interpolants on Powell-Sabin partitions. Technical Report IRMAR 04-16, 2004.
- [12] M.J.D. Powell and M.A. Sabin. Piecewise quadratic approximations on triangles. *ACM Trans. Math. Softw.*, 3:316–325, 1977.
- [13] V.L. Rvachev and T.I. Sheiko. R-functions in boundary value problems in mechanics. *Appl. Mech. Rev.*, 48(4):151–188, 1995.
- [14] V. Shapiro and I. Tsukanov. Meshfree simulation of deforming domains. *Comput. Aided Design*, 31:459–471, 1999.
- [15] X. Shi, S. Wang, W. Wang, and R.H. Wang. The C^1 -quadratic spline space on triangulations. Technical Report 86004, Dep. Math., Jilin University, Changchun, 1986.

- [16] H. Speleers, P. Dierckx, and S. Vandewalle. Local subdivision of Powell-Sabin splines. *Comput. Aided Geom. Design*, accepted, 2006.
- [17] H. Speleers, P. Dierckx, and S. Vandewalle. Numerical solution of partial differential equations with Powell-Sabin splines. *J. Comput. Appl. Math.*, 189(1-2):643–659, 2006.
- [18] E. Vanraes, J. Maes, and A. Bultheel. Powell-Sabin spline wavelets. *Int. J. Wavelets Multires. Information Processing*, 2(1):23–42, 2004.
- [19] K. Willemans and P. Dierckx. Constrained surface fitting using Powell-Sabin splines. In P.J. Laurent, A. Le Méhauté, and L.L. Schumaker, editors, *Proceedings of Wavelets, Images and Surface Fitting*, Second Int. Conf. on Curves and Surfaces, pages 511–520, Chamonix-Mont Blanc, France, 1994. Wellesley.